International Space Planes and Hypersonic Systems and Technologies Conferences
6-9 July 2015, Glasgow, Scotland
20th AIAA International Space Planes and Hypersonic Systems and Technologies Conference

A Comparative Study of Highly Underexpanded Nitrogen and Hydrogen Jets Using Large Eddy Simulation

Xiaopeng Li[1], Kun Wu[2], Wei Yao[3], Xuejun Fan[4]
State Key Laboratory of High Temperature Gas Dynamics, Institute of Mechanics, Chinese Academy of Sciences, Beijing, 100190, P. R. China

The three-dimensional large eddy simulations of highly underexpanded hydrogen and nitrogen jets at the same NPR of 5.60 at Re~10^5 are performed. The flow characteristic for both jets are discussed and compared in detail based on the high resolution LES data. It is found that the H_2 jet mixes more rapidly with the ambient air but has a much smaller mixing area on cross-section planes. The classical near-field structures of highly underexpanded jets are well captured by the current LES modeling, and the shape and size of Mach barrel for both jets are very similar and also agree well with the experimental measurement and the previous studies. However, the flow field and the shock structures after the Mach disk differ greatly. The density values in the annular shear layer for H_2 jet are much lower because of its smaller molecular mass. Meanwhile, the H_2 jet has a much longer jet core and more shock cells. In addition, the dominant instability mode is helical for the N_2 jet, but is axisymmetric for the H_2 jet. There are two discrete peaks of f_s=37.086 kHz and f_{2s}=45.695 kHz in the spectrum of the N_2 jet, which are both single helical modes. The spectrum of the H_2 jet is characterized by a fundamental screech frequency of f_s=47.020 kHz and its high order harmonics.

I. Introduction

SCRAMJET engine is one of the most promising propulsive systems for future hypersonic vehicles because of high performance at large Mach number. Usually air entering the combustor is supersonic at flight speeds beyond Mach 5, thus the residence time of the air in a scramjet engine is on the order of milliseconds[1]. The mixing and diffusive combustion of fuel and air in a conventional scramjet engine take place simultaneously in the combustor. Therefore, ensuring fuel-air mixing and subsequently combustion in such a short time is critical to the design of the scramjet engine[2-4].

[1] Ph.D. Student, State Key Laboratory of High Temperature Gas Dynamics, Institute of Mechanics, Chinese Academy of Sciences, lxpyfy@163.com.
[2] Ph.D. Student, State Key Laboratory of High Temperature Gas Dynamics, Institute of Mechanics, Chinese Academy of Sciences, gywukun09@163.com.
[3] Associate professor, State Key Laboratory of High Temperature Gas Dynamics, Institute of Mechanics, Chinese Academy of Sciences,weiyao@imech.ac.cn.
[4] Professor, State Key Laboratory of High Temperature Gas Dynamics, Institute of Mechanics, Chinese Academy of Sciences, Member AIAA. xfan@imech.ac.cn.

In spite of the high price in production, Hydrogen is a very attractive fuel that may help to solve the problem because of its higher efficiencies than conventional hydrocarbon fuels. Hydrogen gives the highest heat release with the shortest kinetic time[5-6], and is already used as fuel in space propulsion due to its high energy release when burning with oxygen and for its high reactivity[7-8]. In addition, Hydrogen does not produce any harmful pollutants like carbon monoxide (CO), carbon dioxide (CO2), or particulate matter during the combustion process, which is environment-friendly. The fuel is generally ejected into the combustor at pressure much higher than the ambient pressure to ensure a good mixing, which results in a highly underexpanded jet[9-12]. As a result, revealing the flow characteristics and understanding the physical mechanism of a highly underexpanded hydrogen jet are conducive to the development of scramjet engine.

Adamson and Nicholls (1959)[9] presented the first structure of a highly underexpanded jet into quiescent air. Ashkenas and Sherman (1965)[10] indicated that near-field structures of highly underexpanded jets are dominated by the nozzle pressure ratio (NPR) and obtained an empirical formula to predict the Mach disk height according to NPR. Over the years, several more experimental studies[11-18] have been conducted, which have resulted in a good understanding of highly underexpanded jet today. However, the knowledge on a highly underexpanded hydrogen jet is still limited since most of the injected gases used in these studies are air or nitrogen. Hydrogen has higher diffusivity and larger nozzle exit velocities due to its much lower molecular weight, which may result in a much different flow field even at the same NPR. In addition, the previous experimental[11-18] and numerical[19-21] studies on highly underexpanded jets mainly provide the time averaged flow properties by using schlieren photographs and Reynolds averaged Navier-Stokes (RANS) methodology respectively. The instantaneous unsteady flow features of a highly underexpanded jet that dominate the mixing processes are still not well revealed. Although large eddy simulation (LES) of an underexpanded hydrogen jet at NPR of 30.0 has been carried out by Gorle *et al*. (2010)[22], their main goal was to verify the jet injection modeling and the in-depth analysis on the instantaneous flow features was not performed. Another numerical analysis of hydrogen underexpanded jets was implemented by Bonelli *et al*. (2013)[23], which concentrated on the effect of real gas assumption on the general wave structures. Their simulation is two-dimensional, and cannot reveal the flow structures of three-dimensional in nature. Therefore, the need for further and systematical research on a highly underexpanded hydrogen jet is obvious.

In the present study, the three-dimensional compressible LES of high pressure gaseous jet through a practical convergent nozzle are performed to investigate the flow characteristics of a highly underexpanded hydrogen jet. The flow field of a nitrogen jet at the same NPR of 5.60 is also provided for comparison. The Reynolds number is around 10^5 based on the flow parameters at the nozzle exit. A well-designed, hexahedral and block-structured grid containing about 27.3M computational cells is applied. The simulations are carried out using the supersonic compressible flow solver, astroFoam, which is developed based on the OpenFOAM C++ library. The time evolution, average jet structure, shock structures, and the dominant instability modes of H_2 jet are discussed in detail, and are also compared with the N_2 jet.

II. Numerical Approach

The three-dimensional, filtered Navier-Stokes equations for the unsteady compressible Newtonian

fluids with heat and species transfer are solved using the density-based compressible solver, astroFoam, which is developed based on the rhoCentralFoam solver distributed with OpenFOAM v2.3.0. OpenFOAM is a C++ code library of classes for developing more advanced CFD codes and has already contained numerous sophisticated solvers and utilities covering a wide range of problems. The rhoCentralFoam solver[24] has been proved to capture the flow discontinuities (e.g. shock waves) with non-oscillatory and low dissipation by solving the convection-diffusion equation using the semi-discrete KT central scheme[25]. However, the rhoCentralFoam solver is limited to single species non-reacting flows in its standard form. The multiple species transport and multi-component diffusion are added to create the astroFoam solver to investigate the gases mixing and reacting flow. In addition, the astroFoam solver solves for sensible enthalpy equation instead of the transport of total energy in rhoCentralFoam solver in order to easily include the chemical reaction and species transport terms. Similar OpenFOAM solvers have been developed to study the subsonic incompressible turbulent flows by Vuorinen *et al.* (2011)[26] and Baba and Tabor (2009)[27] as well as the supersonic compressible turbulent flows by Vuorinen *et al.* (2013)[28] and Fureby *et al.* (2011, 2013)[29-30]. The filtered sub-grid terms are modeled with the sub-grid scale turbulent kinetic energy one-equation model[31], which is integrated in OpenFOAM in the standard form.

A. Computational Geometry and Grid

Previous studies[32-38] indicated that the sound waves originated in the downstream will propagate upstream to change the initial shear layer structures at the nozzle exit, which will influence the development of jet shear layer in the downstream further. However, A priori knowledge of nozzle exit conditions is usually difficult to be obtained in many practical applications. Therefore, the numerical investigation of underexpanded jets requires implementing the practical nozzle geometries to capture the self-sustained acoustic loop correctly. Some example of such endeavors can be found in the LES of supersonic jets by Liu *et al.* (2009)[39] and Dauptain *et al.* (2010)[40].

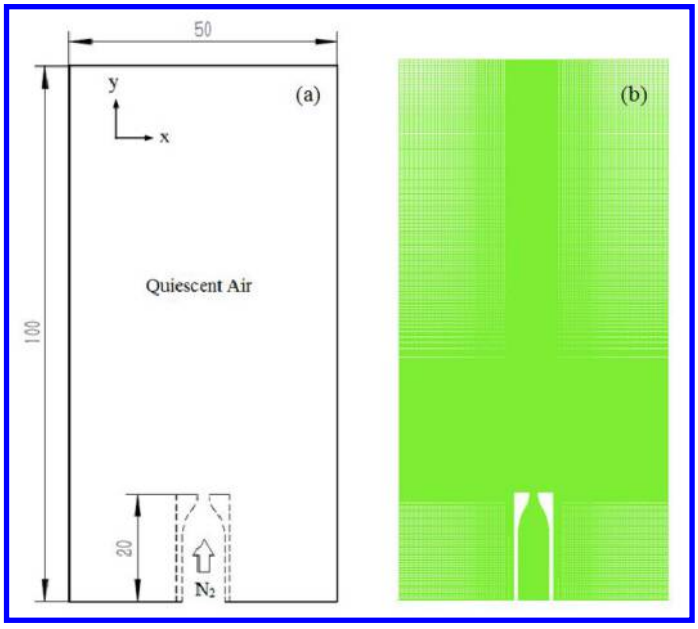

Figure 1. (a) Computational model employed for the LES of highly underexpanded jets (units: mm). (b) Computational grids

The nozzle geometry and the computational domain used in the current LES modeling of underexpanded jets is shown in Figure 1 (a). The computational domain mainly consist of a box of size $50\times100\times50$ mm respectively in x, y, and z directions. The hydrogen or nitrogen jet in the high pressure nozzle (with total pressure P_0 and total temperature T_0) is injected into the quiescent air (with stastic pressure P_∞, and stastic temperature T_∞) from a convergent nozzle of 20.0mm in height. The entrance and exit diameter of the nozzle is 8.0mm and 2.0mm respectively.

Table 1. Grid resolution comparison in the near field (r/D:-1.5~1.5; y/D: 0~5D) of jets in the present and previous LES modeling of supersonic jets.

Grid	D(mm)	Δr_{min}	Δr_{max}	Δy_{min}	Δy_{max}	Re	Total($\times10^6$)
Present work	2.0	D/200	D/52	D/67	D/25	~10^5	27.3
Liu et al. (2009)[39]	72.8	D/29	D/29	D/29	D/29	~10^5	11.0
Dauptain et al. (2010)[40]	25.4	D/35	D/30	D/35	D/30	~10^6	22.0
Rana et al. (2011)[43]	4.0	D/33	D/33	D/33	D/33	~10^4	9.2
Vuorinen et al. (2013)[28]	1.4	D/70	D/50	D/35	D/25	~10^5	12.0

Previous studies[28, 39-43] have indicated that the spatial resolution in LES of supersonic jets need to be rather high. The hexahedral, block-structured grid presented in Figure 1(b) is applied in the current LES modeling. Altogether the mesh contains 27.3M computational cells. The jet core is meshed with high resolution by adding a refinement region which covers the jet core and the jet shear layers. With these careful arrangements, the grid resolution in the main region of interest in this study is similar as those used in the previous LES of supersonic jets[28, 39-40, 43], which are summarized in Table 1. In addition, very coarse cell sizes with a resolution of 1.0 mm in the far field and 0.5 mm at outflow boundaries are used to introduce additional dissipation and avoid wave reflections from these boundaries.

The computational time step is approximately $\Delta t \approx 1.37\times10^{-8}$s ($\Delta t \cdot a / D = 2.42\times10^{-3}$, a is the speed of sound at the nozzle exit) in the present study, which is limited by a maximum Courant-Friedrichs-Lewy (CFL) number of 0.6. This time step has the same order of magnitude with the value that Kawai and Lele (2010)[41] and Génin and Menon (2010)[42] used in their LES modeling of a sonic jet in supersonic cross flow (JISC).

B. Initialization and Boundary Conditions

The quiescent air is the mixture of nitrogen 0.76699 and oxygen 0.23301 by weight, and initially the temperature, pressure, density, and velocity are respectively set as uniform, i.e. T_∞=300K, P_∞=101325Pa, $\rho_\infty = 1.17\text{kg/m}^3$, U_∞=0. The hydrogen and nitrogen jets are injected into the quiescent air with the same total pressure and total temperature at NPR of 5.60, which are typically highly underexpanded jets according to the definition by Donaldson and Snedeker (1971)[12]. The flow conditions at the nozzle exit are close to the sonic speed, and are marked with subscript 1 and summarized in Table 2 in detail.

The inflow at the nozzle inlet is subsonic and the stagnation condition for temperature and pressure is employed, while a zero-gradient condition for velocity is used. All walls including the sides of nozzle and the round tube outside the nozzle are all treated as no-slip adiabatic walls. At the top of the

computational domain together with the four free surfaces of the box, an open boundary condition is applied, i.e. all flow parameters are treated as zero-gradient for outflow and set as ambient values when the backflow occurs.

Table 2 Jet exit flow properties at the sonic orifice

Property	Symbol	Case		Units
		N_2	H_2	
Mach number	M_1	1.0	1.0	-
Static pressure	P_1	0.3	0.3	MPa
Stagnation pressure	P_0	0.57	0.57	MPa
Stagnation temperature	T_0	360.0	360.0	K
Nozzle pressure ratio (NPR)	P_0/P_∞	5.60	5.60	-
Static pressure ratio	P_1/P_∞	2.96	2.96	-
Ratio of specific heats	r	1.4	1.4	-
Molecular Weight	W	28	2	g/mol
Velocity at nozzle exit	U_1	353.1	1321.3	m/s
Density	ρ_1	3.37	0.24	kg/m^3
Reynolds number at nozzle exit	Re_1	1.36	0.72	$\times 10^5$
Nozzle density ratio (NDR)	ρ_1/ρ_∞	2.87	0.21	-
Mass flow rate	$\dot{m}$	3.734	0.998	g/s

The integral time scale is defined using D and the maximum velocities in the near field of the jets as $t_0=D/2U_1\approx 2.5\times10^{-6}$ s. The flow-through time (FTT) for the jets washing out the whole computational domain in streamwise direction is about $t_{total}\approx 0.5ms=200t_0$, thus the total simulation duration is set as $4t_{total}=2.0ms=800t_0$, which is four times the value used by Vuorinen *et al.* (2013)[28] to ensure statistical steady. The instantaneous results are saved every $2t_0$, then turbulent statistics are collected for the last three flow-through times ($200t_0$~$800t_0$, total 300 time steps).

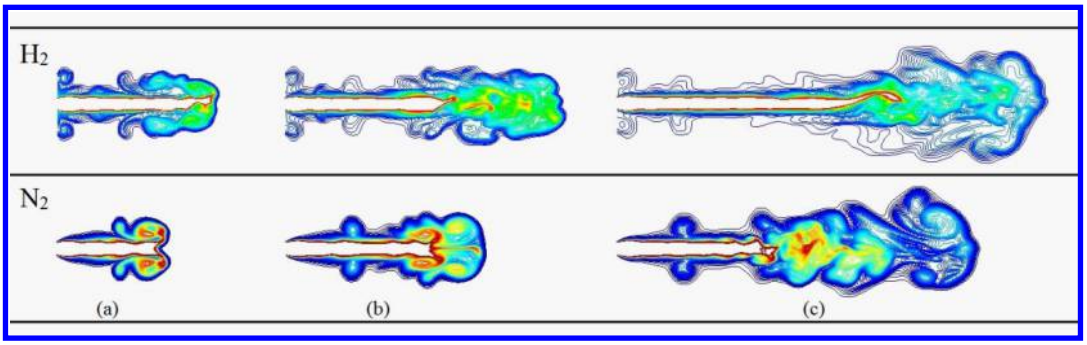

Figure 2. Time evolution of mass fraction Y_s on the midline plane for H_2 and N_2 jets. The instants are successively: (a)$t/t_0=36$, (b)$t/t_0=64$, and (c) $t/t_0=128$, and respectively correspond to the initial phase, the transition phase, and the fully developed flow

III. Results and Discussion

A. Flow Evolution

The temporal evolution of mass fraction for H_2 and N_2 jets at the same NPR of 5.60 is presented in

Figure 2. As can be seen, the main flow structures at different time for hydrogen jet are similar to that of the nitrogen jet. For example, the initial tip vortex ring which is usually visible in subsonic jets and the undulating vortex ring are noted for both the H_2 and N_2 jets. The turbulent transition of the jets is both characterized by the breakdown of recirculation zones, the loss of the flow symmetry, and the generation of streamwise vortexes. Meanwhile, the large-scale turbulent vortices along the jet shear layer are also observed when the jets are fully developed. However, there is a vortex ring near the nozzle exit for the hydrogen jet, which differs from the nitrogen jet.

In addition, the sonic conditions for H_2 and N_2 jets under the same total pressure and total temperature differ greatly due to the differences in the molecular weight. In particularly, Table 2 indicates that velocity at nozzle exit for hydrogen jet is 1321.3m/s, which is much larger than that of 353.1m/s for nitrogen jet. Thereby, the H_2 jet penetrates somewhat faster than the respective N_2 jet.

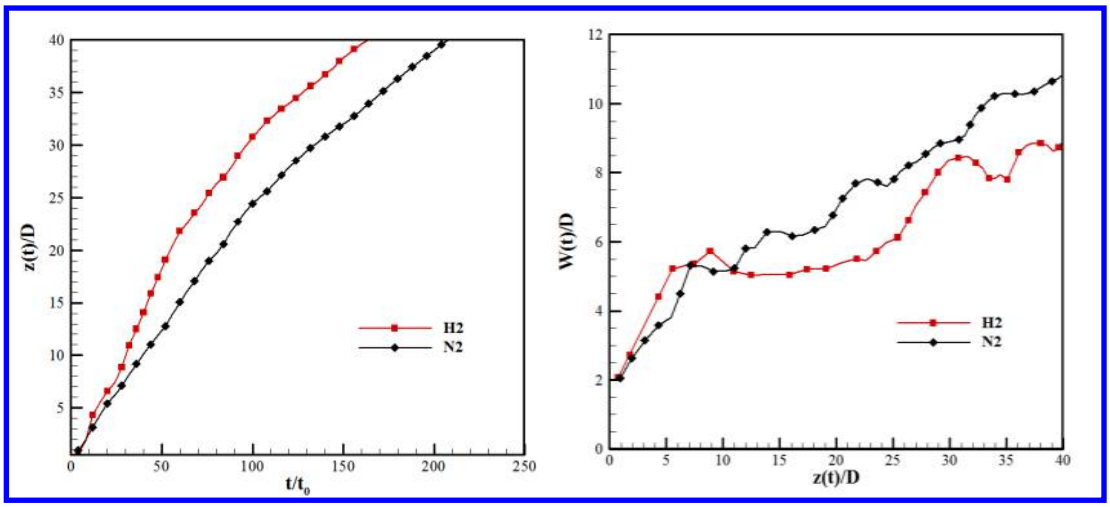

Figure 3. (a)right: Non-dimensional jet penetration rates, (b) left: jet maximum width

The jet penetration $z(t)$ and maximum width $W(t)$ are two important overall parameters to characterize the flow evolution characteristics, and are closely related to the overall mixing and entrainment. In the present study, the jet penetration and maximum width are defined according to the outer limit of mass fraction Y_s on the midline plane. In other words, the jet penetration $z(t)$ is defined as the maximum axial position, and the jet maximum width is defined as the maximum span in the radial direction. The jet penetration $z(t)$ and maximum width $W(t)$ for H_2 and N_2 jets as a function of time are compared quantitatively in Figure 3. Figure 3(a) further confirms the conclusion that the H_2 jet penetrates faster than the N_2 jet. This observation implies that the H_2 jet mixes more rapidly with the ambient air than the respective N_2 jet. However, Figure 3(b) indicates that the jet maximum width for H_2 jet is generally smaller than that of N_2 jet, which will result in a smaller mixing area and is not good for the fuel-air mixing.

B. Average Jet Structure

Figure 4 shows the average streamwise velocities on the centerline plane for H_2 and N_2 jets. As can be seen, the jets are expanded rapidly after injected from the high pressure nozzle, and reach the largest velocity in the vicinity of the Mach disk. The maximum velocity for H_2 jet is around 2600m/s, which is much larger than the 700m/s for N_2 jet. Note that these peak velocities in the Mach disk region are nearly double of the velocities at the nozzle exit U_1 for both jets. After the Mach disk, the general

velocity patterns are very similar and momentum becomes distributed along the annular regions for both jets. However, the potential core of H_2 jet seems to be much longer than that of N_2 jet, which implies that there is may be much more shock cells in H_2 jet.

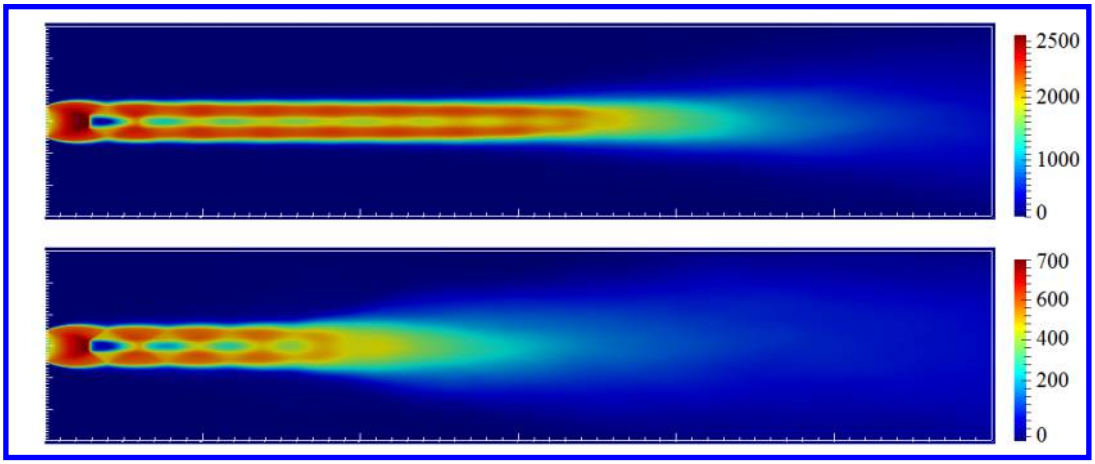

Figure 4. Time averaged contours of streamwise velocities of underexpanded jets on the centerline plane. (a) top: H_2 jet, (b) bottom: N_2 jet

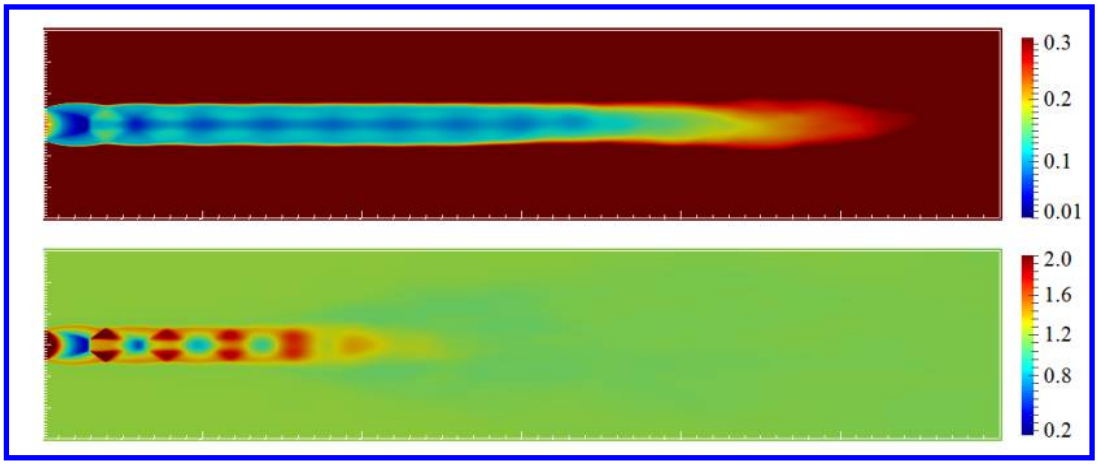

Figure 5. Time averaged contours of density of underexpanded jets on the centerline plane. (a) top: H_2 jet, (b) bottom: N_2 jet

Figure 5 shows the effect of fuel properties on the general density landscape insides the jets. In particularly, great differences are observed in the annular shear layer where the N_2 jet has much higher density values than the H_2 jet. This is understandable since the density of H_2 jet is lower than that of N_2 jet at fully expanded conditions with the same initial pressure and temperature, which is indicated by Table 2. The density at the nozzle exit for N_2 jet is 3.37kg/m^3, which is higher than the ambient value ρ_∞=1.17kg/m^3. On the contrary, the lower molecular mass of H_2 leads to a less dense jet with density of 0.24kg/m^3 at the nozzle exit, which is much lower than the ambient value ρ_∞. The large differences in density for H_2 jet with the ambient air will result in the intense flow discontinuities along the jet shear layer as seen in Figure 6(a). In contrast, the peak values of density gradient in N_2 jet are generally consistent with the shock structures in the flow field, which is shown in Figure 6(b).

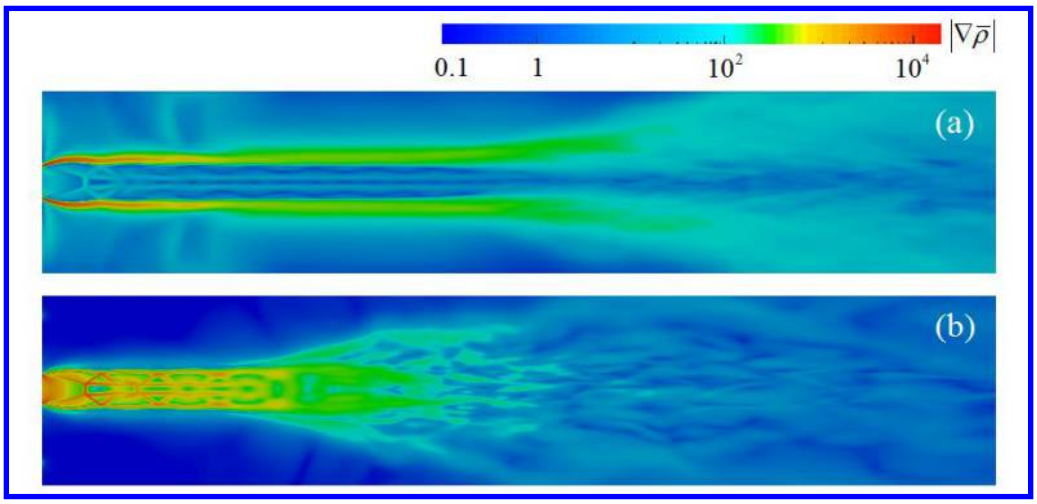

Figure 6. Time averaged density gradient on the centerline plane. (a) H_2 jet, (b) N_2 jet

In addition, the axial density values for N_2 jet after the shock-containing field (around y/D=10) remain higher than the ambient values, so the density along the jet centerline decrease to ρ_∞ gradually after the breakdown of the jet core, which is shown in Figure 7. On the other hand, the axial density of H_2 jet increases almost linearly from around y/D=15 where is near the end of the jet core.

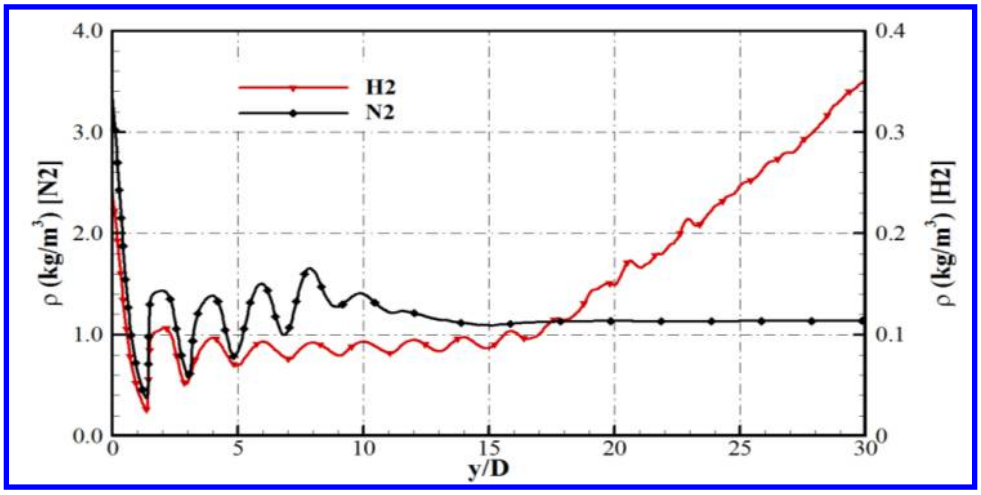

Figure 7. Mean profiles of density along the jet centerline

C. Shock Structures

Figure 8(a) present near field structures for N_2 jet in terms of the time averaged density gradient ($\log_{10}(|\nabla\bar{\rho}|)$) obtained by the current LES modeling. The classical wave structures in the near field of a highly underexpanded jet including the Mach disk, barrel shock, triple point, reflected shock and the slip lines which have been confirmed by the previous experimental studies[9-12, 16-18] and numerical work[19-23, 28] are all well captured by the current LES modeling. In addition, Figure 8(b) shows the schlieren photography of the highly underexpanded nitrogen jet at same NPR of 5.60 measured by Yang (2012)[44] over an exposure time of 0.6 ms. As can be seen, very good agreements of flow structures in the region y/D<5 can be observed.

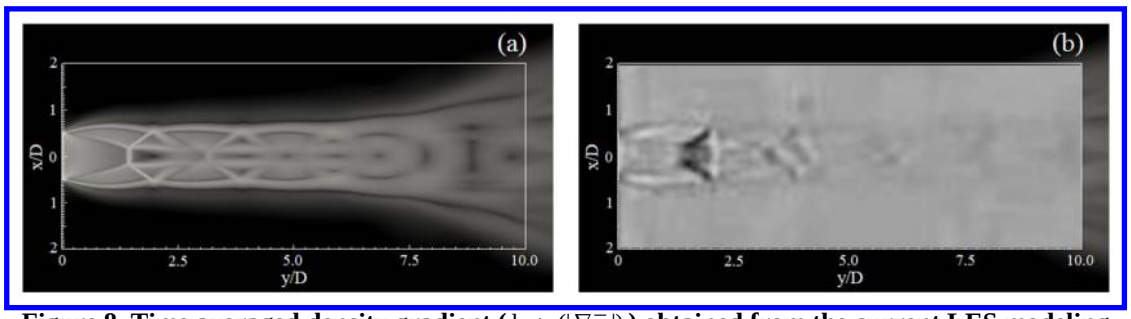

Figure 8. Time averaged density gradient ($\log_{10}(|\nabla\bar{\rho}|)$) obtained from the current LES modeling (a) and schlieren photography[44] (b) for N2 jet at NPR of 5.60

Ashkenas and Sherman (1965)[10] obtained an empirical formula as $H_{\text{disk}} / D = C_H \cdot \sqrt{\text{NPR}}$ to predict the Mach disk height at NPR from 20 to 200. C_H is a constant of 0.67. Ewan and Moodie (1986)[45] observed experimentally a much smaller value of $C_H \approx 0.55$ for NPR<10. Figure 9(a) presents the time averaged profiles of pressure along the jet centerline for H_2 and N_2 jets, and it can be seen that the locations of the first normal shock, i.e. the Mach disk, for both jets are highly overlapped. The corresponding C_H value is 0.61, which is between 0.55 and 0.67 yet close to 0.62 obtained by Vuorinen *et al.* (2013)[28] at similar NPR of 5.5 using LES technique.

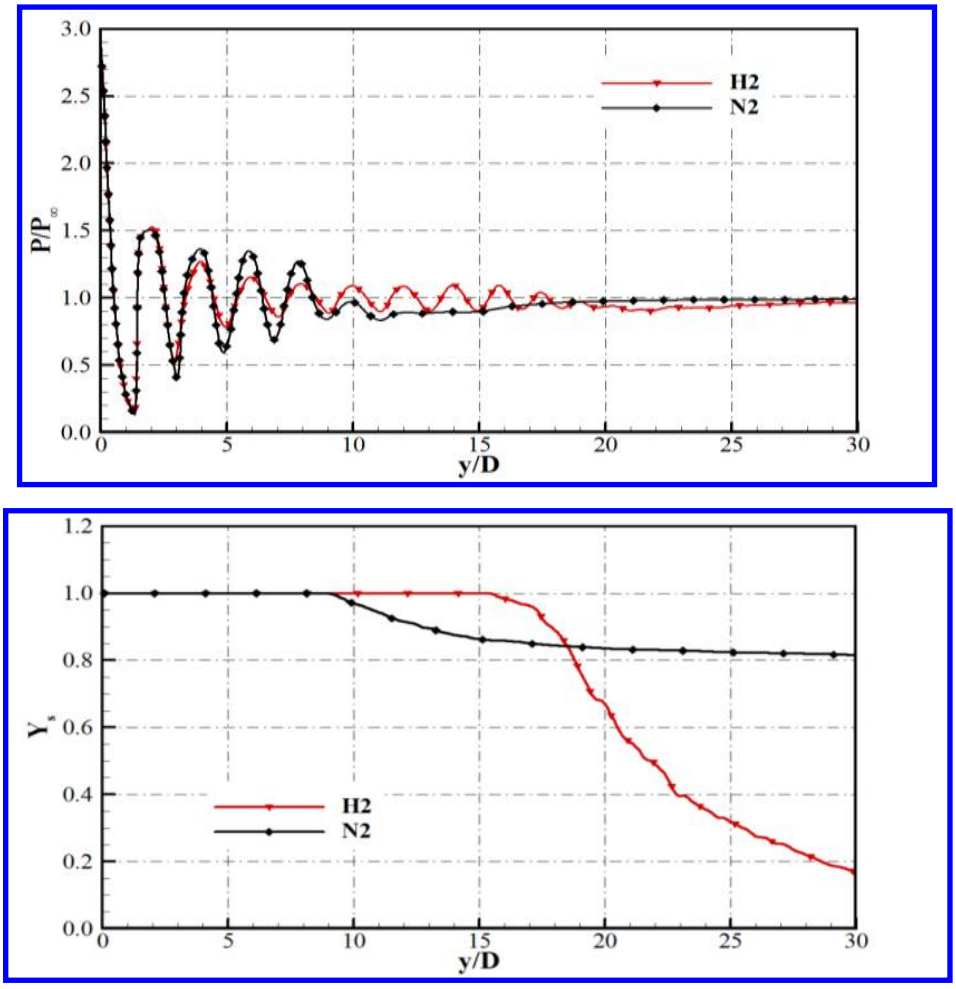

Figure 9. Mean profiles of pressure and fuel mass fraction Y_s along the jet centerline. (a) top: pressure, (b) bottom: mass fraction Y_s

The mean profile of fuel mass fraction shown in Figure 9(b) indicates that the H_2 jet has a much longer jet core of about 15D than that of around 9D for N_2 jet. This is consistent with the previous observations based on the streamwise velocity and density field. More interestingly, Figure 9 demonstrates that the shock structures differ greatly in the jet core for H_2 and N_2 jets although the locations of the Mach disk are highly overlapped. In particularly, the locations of shocks for both jets are not matched anymore after the Mach disk, and there are more shock cells in the H_2 jet. Nine shock cells can be identified in H_2 jet from Figure 9(a), while there are only five shock cells in the N_2 jet. It is also observed that the strength of quasi-periodic shocks after the Mach disk in the H_2 jet is weaker than that in the N_2 jet. This finding implies that the structure and size of Mach barrel of a highly underexpanded jet is mainly dominated by the NPR as indicated by Ashkenas and Sherman (1965)[10] previously. However, the flow field and shock structures after the Mach disk in a highly underexpanded jet may be affected strongly by the injected fuel properties.

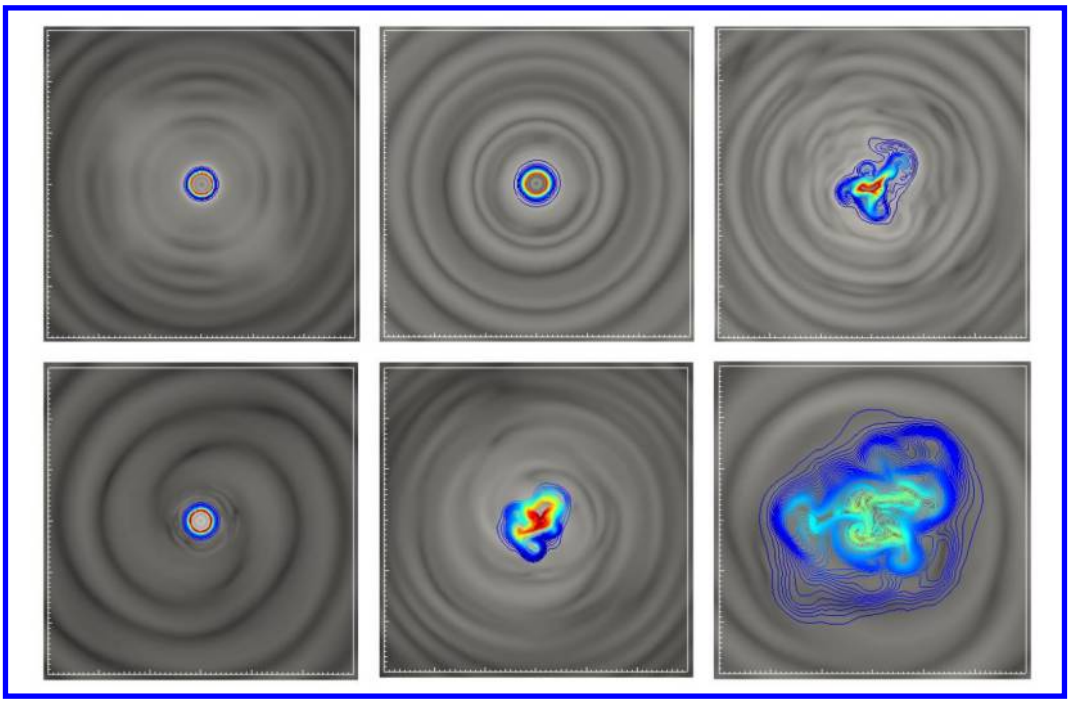

Figure 10. Instantaneous snapshots of density gradient magnitude and contour lines of fuel mass fraction Y_s on the cross-section planes of different streamwise positions. The top and bottom rows represents the H_2 and N_2 jets respectively. The streamwise positions are located at y/D=2(left column), y/D=10(middle column), and y/D=20(right column).

D. Dominant Instability Modes

Powell (1953)[32] observed experimentally that the supersonic underexpanded jets will produce screech tone that dominates all other noise sources in the forward direction. This behavior was attributed to the establishment of an acoustic feedback formed of sound waves that were originated in the downstream due to shock/shear layer interaction, and then propagated upstream to force the initial shear layer at the nozzle lip to generate new structures in the shear layer[32]. Gutmark *et al.* (1989)[34] and Powell *et al.*(1992)[35] found experimentally the dominant instability modes of supersonic screeching jets were affected strongly by NPR. In particularly, Powell *et al.*(1992)[35] indicated that the screech tone

of underexpanded circular jets changes successively from an axially symmetric one to a flapping one, a helical one, and finally a sinuous one as NPR increases from 2.0 to 5.84. Tam *et al.* (1992)[33, 36-37] also derived the following formula to predict the shock screech frequency for a underexpanded jet of Mach number M_j:

$$St = \frac{f_s D_j}{U_j} = \frac{0.67}{(M_j^2 - 1)^{1/2}} \left[1 + \frac{0.7 M_j}{[1 + (\gamma - 1) M_j^2 / 2]^{1/2}} \left(\frac{T_0}{T_\infty} \right)^{1/2} \right]^{-1} \quad (1)$$

where St is the Strouhal number, f_s is the fundamental screech frequency. M_j is the fully expanded jet Mach number, and U_j is the fully expanded jet velocity, both of which can be calculated based on NPR according to the one-dimensional isentropic equations. D_j is the fully expanded jet diameter[33, 36-37]. However, the effects of fuel properties on the dominant instability modes or screech frequency of supersonic underexpanded jets are rarely investigated.

The instantaneous density gradient on different cross-section planes of N_2 jet shown in Figure 10 presents an obvious helical distribution, which implies that the N_2 jet is dominated by the helical mode. However, it is very interesting to find that the density gradient pattern looks like axisymmetric for H_2 jet, which indicates that the dominant screech tone of H_2 jet is axisymmetric mode. In addition, Figure 10 also demonstrates intuitively that the N_2 jet has a much larger mixing area in the downstream than the H_2 jet in terms of the contour lines of fuel mass fraction.

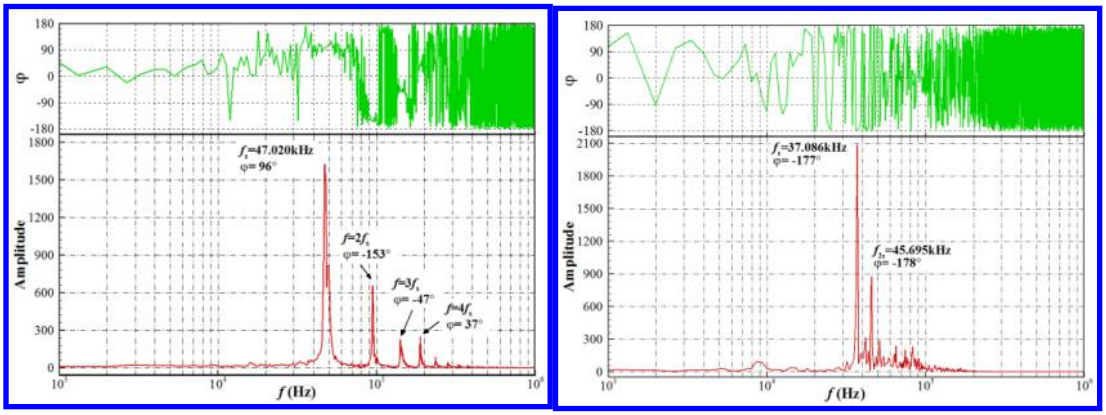

Figure 11. The cross spectrum and relative phase of pressure fluctuation on either side of the jets at (x/D=1, y/D=6, z/D=0) and (x/D=-1, y/D=6, z/D=0). The red lines indicate the amplitude while the green lines indicate the phase φ. (a) left: H_2 jet, (b) right: N_2 jet

Fast Fourier Transformation (FFT) of pressure fluctuation on either side of the jets in (x/D=1, z/D=0) and (x/D=-1, z/D=0) near the jet shear layer for different streamwise positions at y/D=2, 4, 6, 8, 10, 15 are implemented, and Figure 11 shows the spectrum and relative phase at y/D=6 for an example. As can be seen, the N_2 jet has two discrete peaks. One is f_s=37.086 kHz, and the other is f_{2s}=45.695 kHz. The phase angles φ for these two peak frequencies are -177° and -178° respectively, and are both close to π and corresponding to the single helical modes. This is consistent with the previous observation based on the instantaneous density gradient shown in Figure 10. However, the spectrum for H_2 jet differs greatly. The H_2 jet has a much high peak frequency of f_s=47.020 kHz. It is also found that there is some harmonics in the spectrum of H_2 jet. In particularly, it can be clearly identified the first harmonics ($2f_s$), the second harmonics ($3f_s$), and the third harmonics ($4f_s$) at y/D=6 in H_2 jet. The longer

jet core and the more shock-cell structures in H_2 jet are believed to be the main reason to cause the harmonics. But note that the phase angles for the fundamental screech frequency f_s and the high order harmonics in H_2 jet are rather elusive, neither close to 0° nor close to 180°.

In addition, the Strouhal number based on the second peak frequency f_{2s}=45.695 kHz for N_2 jet is 0.202, which is 8.2% smaller than the prediction of 0.220 by the right part of Equation (1). In contrast, the Strouhal number based on the fundamental screech frequency f_s=47.020 kHz for H_2 jet is 0.208, and is 5.4% smaller than the empirical prediction by Equation (1).

IV. Conclusion

In this study, large eddy simulations of highly underexpanded hydrogen and nitrogen jets at the same NPR of 5.60 are carried out using a supersonic compressible OpenFOAM solver. The effects of fuel properties on the flow characteristic of the jets are studied in detail. The main findings of the study are summarized as follows. (1) The injected fuel has a relatively large influence on the mixing properties of jets. The H_2 jet mixes more rapidly with the ambient air than the N_2 jet, but has a much smaller mixing area on cross-section planes. (2) The present LES results reproduce the classical near-field structures of highly underexpanded jets. Particularly the Mach disk dimensions for both jets are highly matched, and are also similar to previous studies. (3) At a given NPR, the flow field and the shock structures after the Mach disk are strongly affected by the injected fuel. The H_2 jet has much lower density values in the annular shear layer than the N_2 jet because of the smaller molecular mass. Meanwhile, the H_2 jet has a much longer jet core and more shock cells. (4) The screech tone of underexpanded jets is affected by the injected fuel. The dominant instability mode is helical for the N_2 jet, but is axisymmetric for the H_2 jet. Two discrete peaks of f_s=37.086 kHz and f_{2s}=45.695 kHz that correspond to the single helical mode both exist in the spectrum of the N_2 jet. The spectrum of the H_2 jet is characterized by a fundamental screech frequency of f_s=47.020 kHz and its high order harmonics. The screech frequencies of f_{2s}=45.695 kHz for N_2 jet and f_s=47.020 kHz for H_2 jet agree reasonably with the previous empirical prediction.

Acknowledgments

This project was supported by the National Natural Science Foundation of China under Contractor No.91016005 and 10621202, and LHD Youth Innovative Foundation (0120481111).

References

1. Corin segal. The scramjet engine processes and characteristics. Cambridge University Press, New York, 2009.
2. Keistler, P. G., Hassan, H. A., and Xiao, X. “Simulation of Supersonic Combustion in Three-Dimensional Configurations,” Journal of Propulsion and Power, Vol. 25, No. 6, 2009, pp. 1233-1239.
3. Su-Hee Won, In-Seuck Jeung, Bernard Parent, and Jeong-Yeol Choi. "Numerical Investigation of Transverse Hydrogen Jet into Supersonic Crossflow Using Detached-Eddy Simulation", AIAA Journal, Vol. 48, No. 6 (2010), pp. 1047-1058.
4. Cecere, D., Ingenito, A., Giacomazzi, E., Romagnosi, L., and Bruno, C. “Hydrogen/Air Supersonic Combustion for Future Hypersonic Vehicles,” International Journal of Hydrogen Energy, Vol. 36, No. 18, 2011, pp. 11969-11984.
5. Contreras A, Yiit S, o ̈zay K, Veziroglu TN. Hydrogen as aviation fuel: a comparison with hydrocarbon fuels.

International Journal of Hydrogen Energy 1997;22(10e11):1053e60.

6. White, C. M., Steeper, R. R., and Lutz, A. E., 2006, "The Hydrogen-Fueled Internal Combustion Engine: A Technical Review," Int. J. Hydrogen Energy, 31(10), pp. 1292–1305.
7. Brewer GD. Hydrogen usage in air transportation. International Journal of Hydrogen Energy 1978;3(2):217e29.
8. Winter CJ. Hydrogen in high-speed air transportation. International Journal of Hydrogen Energy 1990;15(8):579e95.
9. T. C. Adamson Jr, J. A. Nicholls. On the Structure of Jets from Highly Underexpanded Nozzles Into Still Air [J]. Journal of the Aerospace Sciences, 1959, 26(1): 16-24.
10. Ashkenas H, Sherman F. Structures and Utilization of Supersonic Free Jets in Low Density Wind Tunnels. NASA Technical Report 1965, No. CR-60423.
11. Crist. S, Sherman. P, Glass. D. Study of the Highly Underexpanded Sonic Jet [J]. AIAA Journal, 1966, 4(1): 68-71.
12. C. D. Donaldson, R. S. Snedeker, A study of free jet impingment. Part 1. Mean properties of free and impinging jets [J]. Journal of Fluid Mechanics, 1971, 45: 281-319.
13. Miyake M, Biwa T, Endoh Y, Shimotsu M, Murakami S, Komoda, T. The Development of High-Output, Highly Efficient Gas Burning Diesel Engines. CIMAC Paper 1983, D11. 2.
14. Hill P. G, Ouellette P. Transient Turbulent Gaseous Fuel Jets for Diesel Engines [J]. Journal of Fluids Engineering, 1999, 121: 93-101.
15. P. Ouellette, P. G. Hill. Turbulent transient gas injections [J]. Journal of Fluids Engineering, 2000, 122: 743-753.
16. K. Bülent Yüceil, M. Volkan Ötügen, Engin Arik. Interferometric Rayleigh Scattering and PIV Measurements in the Near Field of Underexpanded Sonic Jets [C]. 41st Aerospace Sciences Meeting and Exhibit, AIAA 2003-917.
17. André B, Castelain T, Bailly C. Experimental exploration of underexpanded supersonic jets [J]. Shock Waves, 2013, 24(1): 21-32.
18. Daniel Edgington-Mitchell, Damon R. Honnery, and Julio Soria. The underexpanded jet Mach disk and its associated shear layer [J]. Physics of Fluids (1994-present) 26, 096101 (2014); doi: 10.1063/1.4894741.
19. Otobe Y, Kashimura H, Matsuo S. Influence of nozzle geometry on the near-field structures of a highly underexpanded sonic jet [J]. Journal of Fluids and Structuress, 2008, 24(2): 281-293.
20. Menon N, Skews B. W. Shock wave configurations and flow structures in non-axisymmetric underexpanded sonic jets [J]. Shock Waves, 2010, 20(3): 175-190.
21. Hatanaka K, Saito T. Influence of nozzle geometry on underexpanded axisymmetric free jet characteristics [J]. Shock Waves, 2012, 22(5): 427-434.
22. Gorle C, Gamba M, Ham F. Investigation of an Underexpanded Hydrogen Jet in Quiescent Air Using Numerical Simulations and Experiments. Center for Turbulence Research Annual Research Briefs, Center for Turbulence Research, Stanford, CA, 2010.
23. Francesco Bonelli, Annarita Viggiano and Vinicio Magi. A Numerical Analysis of Hydrogen Underexpanded Jets Under Real Gas Assumption. Journal of Fluids Engineering. Volume 135. Issue 12. 121101.
24. C.J. Greenshields, H.G. Weller, L. Gasparini, J.M. Reese. Implementation of semi-discrete, non-staggered central schemes in a collocated, polyhedral, finite volume framework, for high-speed viscous flows [J]. International Journal of Numerical Methods in Fluids, 2010, 63: 1-21.
25. A. Kurganov, E. Tadmor. New high-resolution central schemes for nonlinear conservation laws and

convection–diffusion equations [J]. Journal of Computational Physics, 2001, 160: 241-282.

26. Ville Vuorinen, Armin Wehrfritz, Jingzhou Yu, Ossi Kaario, Martti Larmi and Bendiks Jan Boersma. Large-eddy simulation of subsonic jets [J]. Journal of Physics: Conference Series, 2011, 318(3): 032052.
27. Baba-Ahmadi MH, Tabor G. Inlet conditions for les using mapping and feedback control [J]. Computers and Fluids, 2009, 38(6): 1299-1311.
28. La Vuorinen V, Yu J, Tirunagari S. Large-eddy simulation of highly underexpanded transient gas jets [J]. Physics of Fluids, 2013, 25(1): 016101.
29. C. Fureby, M. Chapuis, E. Fedina, S. Karl. CFD analysis of the HyShot II scramjet combustor [J]. Proceedings of the Combustion Institute, 2011, 33(2): 2399-2405.
30. M. Chapuis, E. Fedina, C. Fureby. A computational study of the HyShot II combustor performance [J]. Proceedings of the Combustion Institute, 2013, 34(2): 2101-2109.
31. Chakravarthy V, Menon S. Large eddy simulations of turbulent premixed flames in the flamelet regime [J]. Combustion Science and Technology, 2001, 162: 175-222.
32. Powell A. On the mechanismo f chokedj et noise [J]. Proceedings of the Physical Society. Section B, 1953, 66(12): 1039-1056.
33. C.K.W. Tam, J.M. Seiner, J.C. Yu. Proposed relationship between broadband shock associated noise and screech tones [J]. Journal of Sound and Vibration, 1986, 110(2): 309-321.
34. Gutmark E, Schadow K. C, Bicker C. J. Mode switching in supersonic circular jets [J]. Physics of Fluids, 1989, 1(5): 868-873.
35. Powel1 Alan, Yoshikuni Umeda, Ryuji Ishii. Observations of the oscillation modes of choked circular jets [J]. The Journal of the Acoustical Society of America, 1992, 92(5): 2823-2836.
36. C K W Tam. Supersonic jet noise [J]. Annual Review of Fluid Mechanics, 1995, 27: 17-43.
37. Raman G. Advances in understanding supersonic jet screech: review and perspective [J]. Progress in aerospace sciences, 1998, 34(1): 45-106.
38. Berland J, Bogey C, Bailly C. Numerical study of screech generation in a planar supersonic jet[J]. Physics of Fluids (1994-present), 2007, 19(7): 075105.
39. Liu J, Kailasanath K, Ramamurti R, et al. Large-eddy simulations of a supersonic jet and its near-field acoustic properties[J]. AIAA journal, 2009, 47(8): 1849-1865.
40. A. Dauptain, B. Cuenot, Y. M. Gicquel. Large-eddy simulation of a stable supersonic jet impinging on flat plate [J]. AIAA, 2010, 48(10): 2325-2337.
41. S. Kawai, K. Lele. Large-eddy simulation of jet mixing in supersonic crossflows [J]. AIAA Journal, 2010, 48: 2063-2083.
42. Génin. F, Menon S. Dynamics of sonic jet injection into supersonic crossflow [J]. Journal of Turbulence, 2010, 11(4): 1-30.
43. Z. A. Rana, B. Thornber, D. Drikakis. Transverse jet injection into a supersonic turbulent cross-flow [J]. Physics of Fluids, 2011, 23: 046103.
44. YANG Meng. High speed pulsed schlieren technology and its application to flow visualization in supersonic combustion [D]. Master's Thesis. Institute of Mechanics, Chinese Academy of Science, 2012. (in Chinese)
45. B. C. R. Ewan and K. Moodie. Structures and velocity measurements in underexpanded jets [J]. Combustion Science and Technology, 1986, 45(5-6): 275-288.

This article has been cited by:

1. Wei Yao, weiyao@imech.ac.cn Chinese Academy of Sciences; Yueming Yuan, yuanym@imech.ac.cn Chinese Academy of Sciences; Xiaopeng Li, lixiaopeng@iet.cn Chinese Academy of Sciences; Jing Wang, wangjing@imech.ac.cn Chinese Academy of Sciences; Xuejun Fan, xfan@imech.ac.cn Chinese Academy of Sciences A comparative study of elliptical and round scramjet combustors by Improved Delayed Detached Eddy Simulation . [Citation] [PDF] [PDF Plus]
2. E.-J. Teh, C.T. Johansen. 2016. Effectof Particle Momentum Transfer on an Oblique Shock Wave / Laminar Boundary Layer Interaction. *Acta Astronautica* . [CrossRef]